

MULTI-WINDOW APPROACHES FOR DIRECT AND STABLE STFT PHASE RETRIEVAL*

RIMA ALAIFARI[†] AND YUNAN YANG[‡]

Abstract. Phase retrieval from phaseless short-time Fourier transform (STFT) measurements is known to be inherently unstable when measurements are taken with respect to a single window. While an explicit inversion formula exists, it is useless in practice due to its instability. In this paper, we overcome this lack of stability by presenting two multi-window approaches that rely on a “good coverage” of the time-frequency plane by the ambiguity functions of the windows. The first is to use the fractional Fourier transform of a *dilated* Gauss function with various angles as window functions. The essential support of a superposition of the ambiguity function from such window functions is of a “daffodil shape”, which converges to a large disc as more angles are used, yielding a much broader coverage in the time-frequency domain. The second approach uses Hermite functions of various degrees as the window functions. The larger the degree, the wider the ambiguity function but with zeros on circles in the time-frequency domain. Combining Hermite functions of different degrees, we can achieve a wide coverage with zeros compensated by the essential support of the ambiguity function from other Hermite windows. Taking advantage of these multi-window procedures, we can stably perform STFT phase retrieval using the direct inversion formula.

Key words. phase retrieval, short-time Fourier transform, stability, direct method

MSC codes. 42-08, 42C99, 45Q05, 49K40

1. Introduction. In many scientific and engineering fields, seeking to reconstruct a signal or image from magnitude measurements alone is a common challenge. In these applications, only the absolute values of a set of linear measurements can be acquired so that phase information is missing. In some instances, the phase cannot be directly measured or the phase measurements are too noisy to be of use. *Phase retrieval* addresses this problem by using computational algorithms that estimate the missing phase data, enabling the full reconstruction of the original signal or object. This technique is essential in areas such as optics, crystallography, and diffraction imaging, where direct phase measurement is often impractical. Specific audio processing applications also require phase retrieval from certain magnitude-only measurements.

In this paper, we focus on a specific instance of phase retrieval, which aims at recovery from magnitude measurements of the *short-time Fourier transform (STFT)*, that we will first introduce: For a given *window function* $g \in L^2(\mathbb{R})$, the linear mapping that takes any function $f \in L^2(\mathbb{R})$ to its short-time Fourier transform (STFT) or *windowed Fourier transform* is defined as

$$(1.1) \quad V_g f(x, y) := \int_{\mathbb{R}} f(t) \overline{g(t-x)} e^{-2\pi i t y} dt.$$

The special case of the STFT with a Gauss window $g(t) = \varphi(t) := e^{-\pi t^2}$ is sometimes referred to as the *Gabor transform*. The STFT enjoys many nice properties such as the fact that it is a linear isometry from $L^2(\mathbb{R})$ to $L^2(\mathbb{R}^2)$ up to the factor $\|g\|_{L^2(\mathbb{R})}$, i.e.,

$$\|V_g f\|_{L^2(\mathbb{R}^2)} = \|f\|_{L^2(\mathbb{R})} \|g\|_{L^2(\mathbb{R})}.$$

Thus, the reconstruction from the STFT is unique and stable, since for any $f_1, f_2 \in L^2(\mathbb{R})$:

$$\|V_g f_1 - V_g f_2\|_{L^2(\mathbb{R}^2)} = \|V_g(f_1 - f_2)\|_{L^2(\mathbb{R}^2)} = \|f_1 - f_2\|_{L^2(\mathbb{R})} \|g\|_{L^2(\mathbb{R})}.$$

*Submitted to the editors on October 10, 2024.

Funding: R. Alaifari acknowledges support through SNSF Grant 200021_184698. Y. Yang acknowledges support from NSF through grant DMS-2409855, Office of Naval Research through grant N00014-24-1-2088, and Cornell PCCW Affinito-Stewart Grant. Part of the research was performed when Y. Yang was an Advanced Fellow at the Institute for Theoretical Studies, ETH Zürich, and received support from Dr. Max Rössler, the Walter Haefner Foundation, and the ETH Zürich Foundation.

[†]Seminar of Applied Mathematics, ETH Zürich, Zürich, Switzerland (rima.alaifari@math.ethz.ch).

[‡]Department of Mathematics, Cornell University, Ithaca, NY, USA (yunan.yang@cornell.edu).

Furthermore, an explicit inversion formula for the STFT can be given [18].

A question well motivated by applications in audio processing and ptychographic imaging is that of recovering f from partial information of its STFT. More precisely, in these applications, one is interested in recovering a signal f from the magnitude of its STFT, i.e., from $|V_g f|$. This is a special case of a phase retrieval problem, also referred to as *STFT (or Gabor) phase retrieval*. Note that this is a *nonlinear* recovery problem. While it is not straightforward to resolve the missing phase information, there is, interestingly, a formula that relates $|V_g f|$ to the *ambiguity function* $\mathcal{A}f$ of f , defined as

$$\mathcal{A}f(x, y) = \int_{\mathbb{R}} f(t + x/2) \overline{f(t - x/2)} e^{-2\pi i t y} dt,$$

which can be more compactly written as

$$\mathcal{A}f(x, y) = e^{\pi i x y} V_f f(x, y).$$

Its relation with the magnitude of the STFT of f is given by (see e.g. [24])

$$(1.2) \quad \mathcal{F}(|V_g f|^2)(y, -x) = \mathcal{A}f(x, y) \cdot \overline{\mathcal{A}g(x, y)} = V_f f(x, y) \cdot \overline{V_g g(x, y)},$$

where \mathcal{F} denotes the two-dimensional Fourier transform on $L^2(\mathbb{R}^2)$, and “ \cdot ” denotes pointwise multiplication. We note that the above equation is a direct consequence of the *orthogonality relations* of the STFT (cf. [16, Theorem 3.2.1.]). Thus, at least in theory, the ambiguity function $\mathcal{A}f$ can be recovered from $|V_g f|$, whenever $\mathcal{A}g$ is non-zero, through

$$(1.3) \quad \mathcal{A}f(x, y) = \frac{\mathcal{F}(|V_g f|^2)(y, -x)}{\mathcal{A}g(x, y)}.$$

We note that if a value $c \in \mathbb{R}$ is known, for which $f(c) \neq 0$, then f can be reconstructed from its ambiguity function via a one-dimensional inverse Fourier transform with respect to the second variable and setting $t = x/2 + c$:

$$(1.4) \quad f(x + c) = \frac{1}{f(c)} \int_{\mathbb{R}} \mathcal{A}f(x, y) e^{2\pi i (\frac{x}{2} + c)y} dy, \quad x \in \mathbb{R},$$

or equivalently,

$$f(x + c) = \frac{1}{f(c)} \int_{\mathbb{R}} V_f f(x, y) e^{2\pi i (x+c)y} dy, \quad x \in \mathbb{R}.$$

In practice, however, this approach is very unstable in general: if the window g is well-localized in either time or frequency, which is the case for meaningful windows, this will be reflected in its ambiguity function $\mathcal{A}g$. More precisely, if, for example, g decays fast in time, then $\mathcal{A}g(x, y)$ will also decay rapidly in the x -direction. The same is true for fast decay of g in frequency, yielding a corresponding decay of $\mathcal{A}g$ in y .

Note that for many applications, it is desirable to work with a window that is well localized in time and frequency because, in this case, the STFT yields a representation of the signal that is better localized in time and frequency, i.e., it can better describe which frequencies occurred (roughly) at what time (with the limit being the uncertainty principle). Hence, even if $\mathcal{A}g$ is nonzero everywhere on \mathbb{R}^2 , its magnitude typically decays very fast, making recovery of $\mathcal{A}f$ via Equation (1.3) highly unstable. Take for example the Gauss window φ . Its ambiguity function is a two-dimensional Gauss function, i.e.,

$$\mathcal{A}\varphi(x, y) = \frac{1}{\sqrt{2}} e^{-\frac{\pi}{2}(x^2 + y^2)},$$

which decays exponentially as $x, y \rightarrow \pm\infty$. Recovery of $\mathcal{A}f$ via pointwise inversion by $\mathcal{A}\varphi$, as Equation (1.3) suggests, is therefore numerically infeasible, unless the signal f itself also happens to be very well-localized in time and in frequency.

The goal of this paper is to propose algorithms that can employ the convenient and explicit inversion formula (1.3) in a way that is numerically stable. Existing reconstruction algorithms are much more involved: the most prominent algorithms employed for a wide range of phase retrieval problems are iterative projection algorithms, such as the Gerchberg–Saxton algorithm [15] and Fienup’s algorithm [14], Averaged Alternating Reflections [7] and its variants [11, 13, 21, 20, 10]. A more recent popular iterative scheme is Wirtinger Flow [8]. There also exist methods based on convex relaxation, such as PhaseLift [9], which is based on the idea of *lifting* the problem to higher dimensions and then recovering a low-rank solution of a linear problem instead of solving the non-linear phase retrieval problem. In practice, however, these algorithms have not been adopted as the iterative methods mentioned before are computationally much more efficient.

Another method, specific to STFT phase retrieval, is phase gradient heap integration (PGHI), which recovers the phase of $V_g f$ point by point along a grid on the time-frequency plane [22]. By far, we have not described the entire literature on phase retrieval algorithms here. For a thorough description, we refer to [12].

In this paper, we propose a different approach to STFT phase retrieval. The idea is to use the simple and explicit inversion formula (1.3) but with measurements with respect to *several* windows instead of one. This way, we can give theoretical guarantees for stability (cf. Section 3).

It is important to emphasize that not only does the specific reconstruction formula (1.3) exhibit poor stability properties when used with a single window function, but Gabor phase retrieval itself (from a single window function) is inherently unstable [4]. The stability properties can be linked to the *connectedness* of the Gabor transform magnitude as a function in the time-frequency plane [18]. Stability can be restored when global recovery of the phase is relaxed and one only aims at recovering the phase on each connected component individually [3]. In this work, we intend to take a different route: instead of drawing measurements from one single window g , we take the STFT magnitudes from *several different windows*. This way, we overcome the trade-off between stability and disconnectedness of the measurements. We aim at *stably* recovering the signal *globally*, instead of on each connected component individually (the latter being inherent to the single window setup). The central question we address in this work is the following:

Question. Suppose we can take the STFT magnitude with respect to several windows $\{g_j\}_{j=1}^N$, obtaining a family of measurements $\{|V_{g_j} f|\}_{j=1}^N$. Can we stably recover f based on the reconstruction formula (1.3) with a collection of properly chosen windows $\{g_j\}_{j=1}^N$?

The rest of the paper is organized to address this key question. In Section 2, we propose two multi-window algorithms for STFT phase retrieval — one utilizing fractionally Fourier transformed dilated Gaussian windows, and the other employing Hermite functions of varying degrees. Section 3 establishes mathematical results on the improved inverse problem stability provided by these two multi-window approaches. In Section 4, we present several numerical examples, and conclusions are drawn in Section 5.

2. Multi-window approaches for STFT phase retrieval. In what follows, we propose a framework to use Equation (1.3) constructively, via employing multiple windows $\{g_j\}_{j=1}^N$ with *different time-frequency concentration* each. This way, each set of phaseless measurements $|V_{g_j} f|$ for a given j allows for stable extraction of a *portion* of $\mathcal{A}f$, with the region of extraction dictated by the decay of $\mathcal{A}g_j$. Hence, by acquiring more measurements, we can patch together the different pieces of $\mathcal{A}f$ and globally recover f . Note that the ambiguity function has its maximum at the origin $(0, 0)$ [16]. Therefore, we cannot create windows with ambiguity functions centered at a point different from the origin.

We propose recipes for stable STFT phase retrieval from multiple windows through the fol-

lowing approach:

For some fixed $\varepsilon > 0$ and a family of windows $\{g_j\}_{j=1}^N$, such that $\{|V_{g_j}f|\}_{j=1}^N$ is measured, proceed as follows:

- For each window g_j , determine the region $\Omega_j \subset \mathbb{R}^2$ such that $|\mathcal{A}g_j| > \varepsilon$ on Ω_j . Choose the Ω_j 's to be pairwise disjoint.
- For each j , recover $\mathcal{A}f$ on Ω_j by employing the measurements $|V_{g_j}f|$ in (1.2).
- Combine these partial reconstructions to a global approximation of $\mathcal{A}f$.
- Reconstruct an approximation of f (up to a constant global phase factor) from the approximation of its ambiguity function $\mathcal{A}f$ through Equation (1.4).

In particular, we propose two architectures for $\{g_j\}_{j=1}^N$. The first is based on *fractional Fourier transforms of dilated Gaussians*, while the second is based on *Hermite functions of different order*. These choices are based on properties of the ambiguity functions of these windows. Before we describe the two measurement systems, we first record some preliminary facts that will be employed.

2.1. Dilated Gauss windows under the fractional Fourier transform. To begin with, we give the definition of the *fractional Fourier transform* (FrFT) \mathcal{F}_α of $f \in L^1(\mathbb{R})$ by the angle α , which will be essential in what follows:

$$\mathcal{F}_\alpha f(y) := c_\alpha e^{\pi i y^2 \cot \alpha} \int_{\mathbb{R}} f(t) e^{\pi i t^2 \cot \alpha} e^{-2\pi i t y / \sin \alpha} dt,$$

when $\alpha \in \mathbb{R} \setminus \pi\mathbb{Z}$. Here, c_α is the square root of $1 - i \cot \alpha$ with positive real part. For angles $\alpha = k\pi, k \in \mathbb{Z}$, the fractional Fourier transform is defined as $\mathcal{F}_{k\pi} f := f$ for k even, and as $\mathcal{F}_{k\pi} f(y) := f(-y)$, for k odd. Note that $\mathcal{F}_{\pi/2} = \mathcal{F}$, i.e., it is the standard Fourier transform. By a classical density argument, the fractional Fourier transform can be extended to all functions in $L^2(\mathbb{R})$ [19].

A property crucial to our first approach is the effect of the fractional Fourier transform on the STFT, which can be described as follows [6]:

$$(2.1) \quad V_{\mathcal{F}_\alpha g} \mathcal{F}_\alpha f(x, y) = V_g f(R_\alpha(x, y)) e^{\pi i \sin \alpha ((x^2 - y^2) \cos \alpha - 2xy \sin \alpha)}, \quad x, y \in \mathbb{R},$$

for $\alpha \in \mathbb{R}$ and $f, g \in L^2(\mathbb{R})$, where $R_\alpha(x, y) = (x \cos \alpha - y \sin \alpha, x \sin \alpha + y \cos \alpha)$, i.e., it is the rotation of the vector $(x, y) \in \mathbb{R}^2$ by the angle α . Thus,

$$|V_{\mathcal{F}_\alpha g} \mathcal{F}_\alpha f(x, y)| = |V_g f(R_\alpha(x, y))|, \quad \text{for } x, y \in \mathbb{R},$$

so that $|V_{\mathcal{F}_\alpha g} \mathcal{F}_\alpha f|$ is a rotation by α of $|V_g f|$.

Let us now consider Gauss functions parameterized by a dilation factor $a > 0$,

$$\varphi^a(t) := a^{1/4} e^{-a\pi t^2},$$

for which $\|\varphi^a\|_{L^2(\mathbb{R})} = 2^{-1/4}$. Computing the ambiguity function of φ^a yields

$$\mathcal{A}\varphi^a(x, y) = \frac{1}{\sqrt{2}} e^{\pi i x y} e^{-\frac{\pi(a^2 x^2 + 2iaxy + y^2)}{2a}} = \frac{1}{\sqrt{2}} e^{-\frac{\pi}{2}(ax^2 + \frac{1}{a}y^2)}.$$

Hence, the radial decay for the standard Gauss $\varphi = \varphi^1$ is replaced by an elliptical decay with the x -axis stretched by the factor a . Next, let $\{\alpha_j = \pi j/N\}_{j=1}^N$ be a set of angles for which we consider the family of window functions

$$\phi_j := \mathcal{F}_{\alpha_j} \varphi^a, \quad 1 \leq j \leq N,$$

for some fixed dilation factor $a > 1$ and some discretization parameter N such that $\{\alpha_j\}_{j=1}^N$ is an equidistant discretization of the interval $[0, 2\pi]$. In view of Equation (2.1), this choice of windows results in ambiguity functions $\mathcal{A}\phi_j$ that have an elliptical exponential decay stretched by a factor a along the axis $(\cos \alpha_j, \sin \alpha_j)$. The superposition of these “essential supports” is shaped in the form of a daffodil and approaches a disc shape by taking N larger, which is also illustrated in Figure 1.

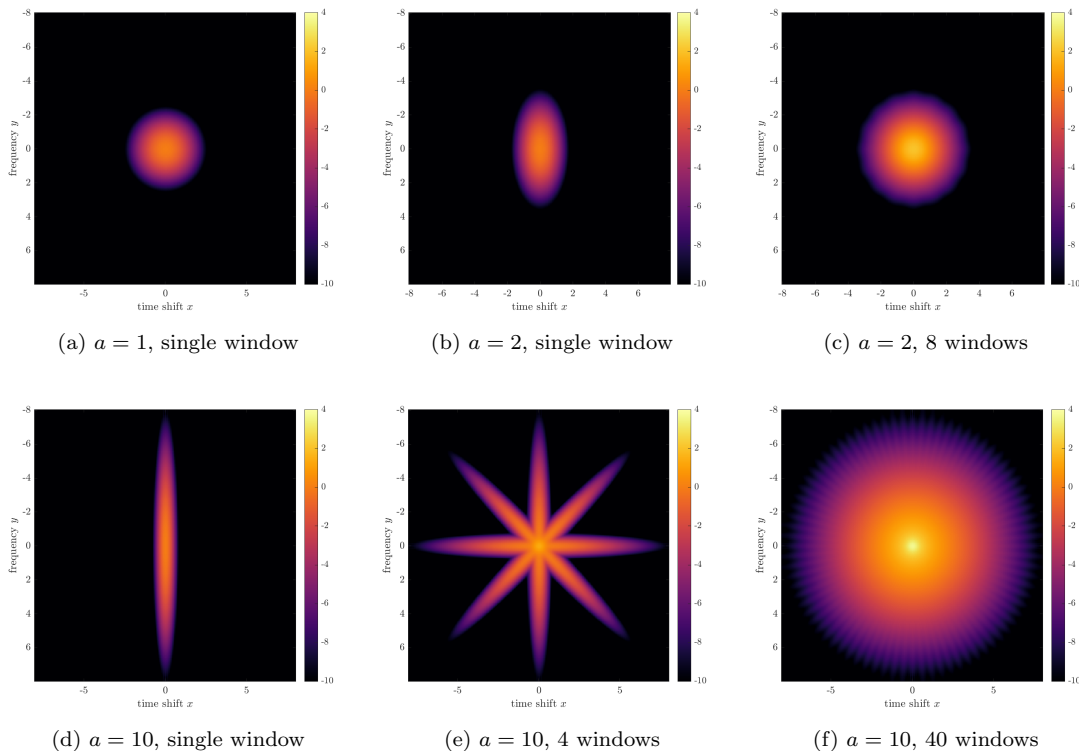


Fig. 1: The absolute value of the sum of multiple fractional Fourier transformed (dilated) Gauss windows plotted in the log scale. (a) $\mathcal{A}\varphi^1$, where φ^1 is the standard Gauss; (b) $\mathcal{A}\varphi^2$ for the dilated Gauss with $a = 2$; (c) $\sum_{j=1}^N \mathcal{A}(\mathcal{F}_{\alpha_j}\varphi^2)$ with $N = 8$; (d) $\mathcal{A}\varphi^{10}$ for the dilated Gauss with $a = 10$; (e) $\sum_{j=1}^N \mathcal{A}(\mathcal{F}_{\alpha_j}\varphi^{10})$ with $N = 4$; (f) $\sum_{j=1}^N \mathcal{A}(\mathcal{F}_{\alpha_j}\varphi^{10})$ with $N = 40$.

Note that the “leaves” of the daffodil grow in length but get narrower in width as a becomes larger. Thus, to approximately cover a disc of a larger diameter, the number of windows N has to grow too. We also remark that the dilated Gauss function is not the only possible choice. The main property that is exploited here, is the fact that the ambiguity functions of these (dilated) Gauss functions have no zeros and are strictly lower bounded on a predefined region (which we choose to be elliptical). A result in [17] states that the Gauss function is not the only window with zero-free ambiguity function. Another example is the *one-sided exponential*.

The daffodil-shaped geometry shown in Figure 1e is a very simple construction and the reconstruction can be further simplified as follows. A simple calculation yields that the ambiguity

functions of ϕ_j are real-valued and positive. Here, we use the notation $R_{\alpha_j}(x, y) = (x(\alpha_j), y(\alpha_j))$:

$$\begin{aligned} \mathcal{A}\phi_j(x, y) &= e^{\pi i x y} V_{\phi_j} \phi_j(x, y) \\ &= e^{\pi i x y} e^{\pi i \sin \alpha_j ((x^2 - y^2) \cos \alpha_j - 2xy \sin \alpha_j)} V_{\varphi^a} \varphi^a(R_{\alpha_j}(x, y)) \\ &= e^{\pi i x(\alpha_j) y(\alpha_j)} V_{\varphi^a} \varphi^a(x(\alpha_j), y(\alpha_j)) \\ &= \mathcal{A}\varphi^a(R_{\alpha_j}(x, y)). \end{aligned}$$

Since $\mathcal{A}\varphi^a$ is real-valued and positive, this is also true for $\mathcal{A}\phi_j$. Therefore, we can directly sum the reconstruction formula (1.2) over $j = 1, \dots, N$:

$$(2.2) \quad \sum_{j=1}^N \mathcal{F}(|V_{\phi_j} f|^2)(y, -x) = \mathcal{A}f(x, y) \cdot \sum_{j=1}^N \mathcal{A}\phi_j(x, y),$$

and determine $\mathcal{A}f$ on the domain

$$\Omega = \left\{ (x, y) \in \mathbb{R}^2 : \sum_{j=1}^N \mathcal{A}\phi_j(x, y) > \varepsilon \right\}$$

through pointwise division in (2.2). We propose [Algorithm 2.1](#) for the multi-window inversion using fractionally Fourier transformed Gaussian windows at various angles.

Algorithm 2.1 A Multiscale STFT Phase Retrieval Algorithm Based on the Fractionally Fourier Transformed Gaussian Windows.

- 1: Given $|V_{\mathcal{F}_\alpha \varphi^a} f|$ and $\mathcal{A}(\mathcal{F}_\alpha \varphi^a)$ where φ^a is the dilated Gaussian, and \mathcal{F}_α denotes the Fractional Fourier transform. We consider measurements from a collection of angles $\{\alpha_j\}_{j=1}^N$ and define $\phi_j = \mathcal{F}_{\alpha_j} \varphi^a$. Let ε be the tolerance.
 - 2: **for** $j = 1$ to N **do**
 - 3: Compute $\phi_j(x, y) = \mathcal{F}(|V_{\phi_j} f|^2)$ (2D FFT) and $\tilde{G}_j(x, y) = G_j(y, -x)$.
 - 4: **end for**
 - 5: Find $\Omega = \{(x, y) : \sum_{j=1}^N \mathcal{A}\phi_j > \varepsilon\}$.
 - 6: Define $J(x, y) = \sum_{j=1}^N \tilde{G}_j(x, y) / \sum_{j=1}^N \mathcal{A}\phi_j(x, y)$, for $(x, y) \in \Omega$ and $J(x, y) = 0$ on Ω^c .
 - 7: Compute $\hat{J}(x, \cdot) = \mathcal{F}^{-1}(J(x, \cdot))$ (1D FFT).
 - 8: Return the reconstructed signal $\tilde{f}(x+c) = \hat{J}(x, x/2+c) / \overline{f(c)}$ (assuming $f(c) \neq 0$).
-

A drawback of this setup is that many windows are required to achieve a good support coverage of the time-frequency plane by their ambiguity functions, such as the disc shown in [Figure 1f](#). Next, we propose a more technical construction, but with the advantage of requiring less data in the sense that fewer windows are necessary for a good support coverage.

2.2. Hermite windows. For this second architecture, the set of windows will consist of Hermite (also called Hermite–Gaussian) functions of increasing order. Their ambiguity functions have rotational symmetry with a number of circular root sets related to the order of the Hermite function; see [Figures 2a to 2c](#). The idea of our approach is to recover $\mathcal{A}f$ as if one was “peeling an onion”: for each Hermite function, we define an annulus on which $\mathcal{A}f$ can be retrieved stably. The union of these annuli results in a large disc in the time-frequency plane. In what follows, we will make this procedure more precise. For this, we start with the definition of the Hermite function h_n of order n [1]:

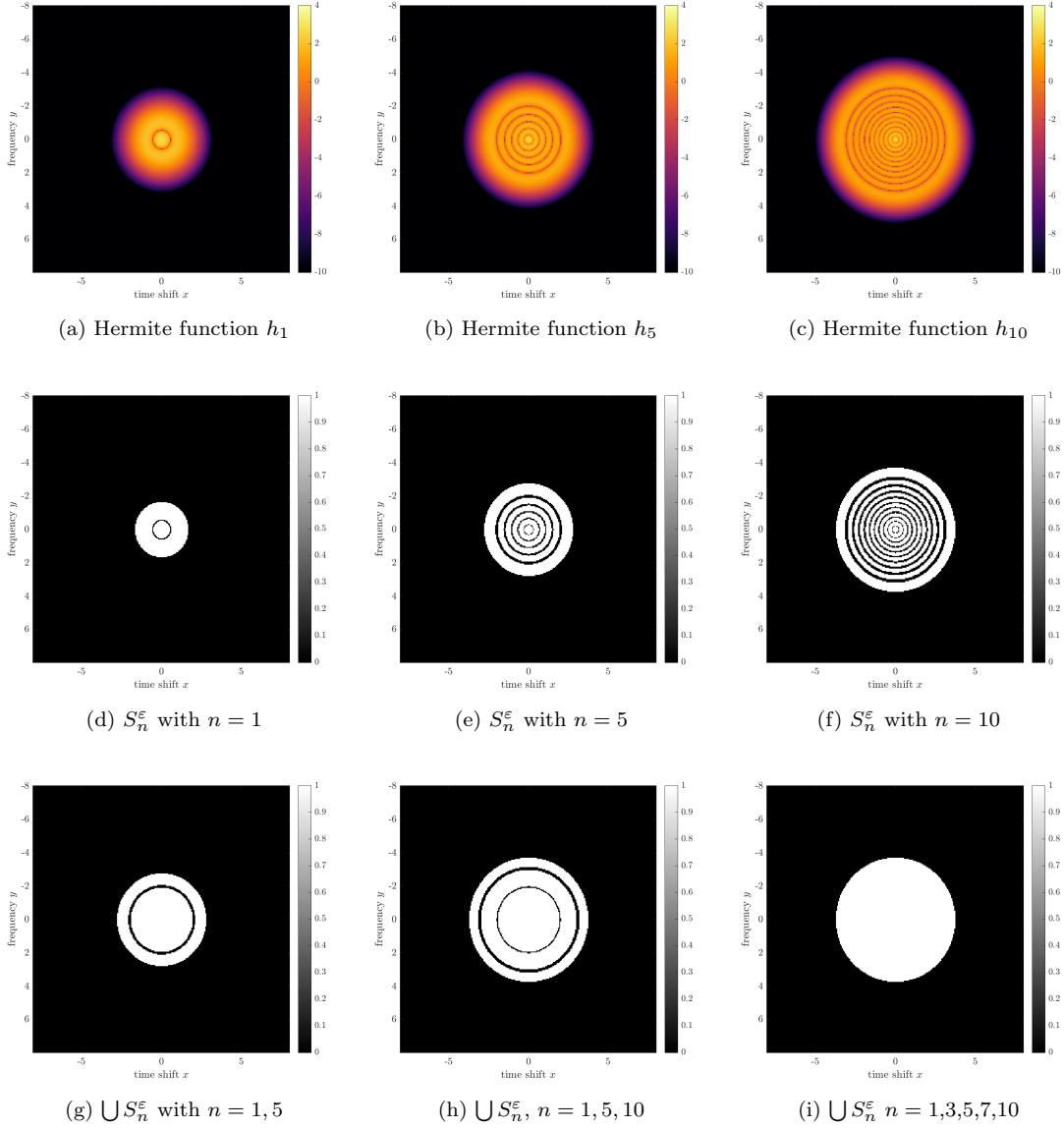


Fig. 2: Top row (a)-(c): the absolute value of the Hermite function ambiguity function plotted in the log scale for $n = 1, 5, 10$, respectively. Middle row (d)-(f): the white region reflects the stability set S_n^ϵ defined in (2.4) with $\epsilon = 0.1$ for Hermite functions of degree $n = 1, 5, 10$, respectively. Bottom row (g)-(i): the white region reflects the union of the stability set $\cup S_n^\epsilon$ in (2.4) with $\epsilon = 0.1$ for Hermite functions with different sets of the indices n .

DEFINITION 2.1. For $n \in \mathbb{N}$, the n -th Hermite function is defined as

$$h_n(t) := c_n e^{\pi t^2} \frac{d^n}{dt^n} e^{-2\pi t^2},$$

where c_n is a constant such that $\|h_n\|_{L^2(\mathbb{R})} = 1$. In particular, $h_0(t) = 2^{1/4} e^{-\pi t^2}$, which is the

L^2 -normalized standard Gauss function.

We summarize a few basic properties of the Hermite functions in the following.

LEMMA 2.2. *The Hermite functions h_n are L^2 -normalized, i.e., $\|h_n\|_{L^2(\mathbb{R})} = 1$ and h_n is the n -th eigenfunction of the Fractional Fourier transform with*

$$\mathcal{F}_\alpha h_n = e^{-i\alpha n} h_n.$$

The family $\{h_n\}_{n \in \mathbb{N}}$ forms an orthonormal basis of $L^2(\mathbb{R})$. In particular, the Fourier transform of h_n is $(-i)^n h_n$.

The ambiguity function of the n -th Hermite function is [5]

$$(2.3) \quad \mathcal{A}h_n(x, y) = e^{-\pi(x^2+y^2)/2} L_n(\pi(x^2 + y^2)),$$

where $L_n(z)$, $z \in \mathbb{R}$, is the Laguerre polynomial

$$L_n(z) := \sum_{k=0}^n \frac{n!}{(n-k)!k!} \frac{(-z)^k}{k!}.$$

We further define the n -th Laguerre function $\mathfrak{L}_n(z)$ as

$$\mathfrak{L}_n(z) = e^{-z/2} L_n(z), \quad z \in \mathbb{R}.$$

The set of Laguerre functions $\{\mathfrak{L}_n(z)\}_{n \in \mathbb{N}}$ forms an orthogonal basis of $L^2(\mathbb{R})$ and

$$\mathcal{A}h_n(x, y) = \mathfrak{L}_n(\pi(x^2 + y^2)).$$

The n -th Laguerre polynomial, and hence also the n -th Laguerre function, has exactly n (strictly positive, pairwise different) roots. By Equation (2.3), $\mathcal{A}h_n$ is rotation-invariant. Hence, the root set of $\mathcal{A}h_n$ consists of n disjoint circles, centered at the origin $(0, 0)$ and thus has Lebesgue measure zero.

When solving the STFT phase retrieval problem with the help of (1.2), the stability of this recovery will be dictated by the absolute value of the ambiguity function: to recover the ambiguity function of the unknown signal via Equation (1.2) requires the division by the ambiguity function of the window. Therefore, this process is very unstable whenever the ambiguity function of the window is small in magnitude. Consequently, we need to understand when $\mathcal{A}h_n(x, y)$, the ambiguity function of the n -th Hermite window, is small in absolute value to avoid such regions in our algorithm.

To this end, we consider the stability set S_n^ε for any $\varepsilon \in (0, 1)$ defined by

$$(2.4) \quad S_n^\varepsilon := \{(x, y) \in \mathbb{R}^2 : |\mathcal{A}h_n(x, y)| > \varepsilon\} = \{(x, y) \in \mathbb{R}^2 : |\mathfrak{L}_n(\pi(x^2 + y^2))| > \varepsilon\}.$$

In Figures 2d to 2f, the white region reflects the set S_n^ε with $\varepsilon = 0.1$ and $n = 1, 5, 10$, respectively. The stability set S_n^ε is determined by the subset of \mathbb{R} on which the n -th Laguerre function \mathfrak{L}_n has a large absolute value. Hence, better estimates of S_n^ε can aid the design of an efficient numerical strategy for phase retrieval by choosing a minimal set of Hermite windows $\{h_{n_k}\}$, such that $\bigcup_k S_{n_k}^\varepsilon$ is as large as possible. As shown in Figures 2g to 2i, we plot the union of the stability set $\bigcup_{n \in I} S_n^\varepsilon$ for different sets of indices I . The larger the set I , the larger the union of the stability sets on which we can stably recover $\mathcal{A}f(x, y)$.

We propose Algorithm 2.2 for the multi-window STFT phase retrieval using Hermite functions of various degrees as the measuring windows.

Remark 2.3. If we are given $V_g g$ rather than $\mathcal{A}g$ where g is the window function, we can still use Algorithms 2.1 and 2.2 with $\mathcal{A}g$ therein replaced by $V_g g$ and the Step 8 of both algorithms changed to $\tilde{f}(x+c) = \widehat{J}(x, x+c)/\overline{f(c)}$, assuming $f(c) \neq 0$.

Algorithm 2.2 A Multiscale Algorithm for the Hermite Functions

-
- 1: Given the phaseless STFT measurements $|V_{h_{n_j}} f|$ and the ambiguity functions $\mathcal{A}h_{n_j}$ where h_{n_j} is the n_j -th Hermite function, $j = 1, \dots, N$, with $n_1 < \dots < n_N$. Let $\Omega = \emptyset$ and the tolerance be $\varepsilon > 0$.
 - 2: **for** $j = 1$ to N **do**
 - 3: Find $\Omega_j = \{(x, y) : |\mathcal{A}h_{n_j}| > \varepsilon\} \setminus \Omega$ and update $\Omega \leftarrow \Omega \cup \Omega_j$.
 - 4: Compute $G_j(x, y) = \mathcal{F}(|V_{h_{n_j}} f|^2)$ (using 2D FFT) and set $\tilde{G}_j(x, y) = G_j(y, -x)$.
 - 5: Define $J(x, y) = \tilde{G}_j(x, y) / \overline{\mathcal{A}h_{n_j}(x, y)}$, for $(x, y) \in \Omega_j$.
 - 6: **end for**
 - 7: Set $J = 0$ on Ω^c . Compute $\hat{J}(x, \cdot) = \mathcal{F}^{-1}(J(x, \cdot))$ (using 1D inverse FFT).
 - 8: Return the recovered function $\tilde{f}(x + c) = \hat{J}(x, x/2 + c) / \overline{\hat{f}(c)}$ (assuming $f(c) \neq 0$).
-

3. Stability estimates. The improved stability properties of our approach, evidenced by numerical examples in Section 4, can be quantified more explicitly. We first derive an estimate for Algorithm 2.1. A simple modification, outlined in Section 3.2, implies a similar result for Algorithm 2.2.

For this, suppose that on each region $\Omega_j \subset \mathbb{R}^2$ we compare a set of *exact* measurements

$$\left\{ F_j := |V_{g_j} f|^2 \right\}_{j=1}^N,$$

and measurements corrupted by additive noise

$$\left\{ F_j^\eta := |V_{g_j} f|^2 + \eta_j \right\}_{j=1}^N,$$

where $\{g_j\}_{j=1}^N$ is a set of N distinct window functions. The goal is to analyze the stability of reconstructing f from $\{F_j\}_{j=1}^N$ via formulas (1.3) and (1.4), where we employ (1.3) with F_j, F_j^η on Ω_j for each $j = 1, \dots, N$.

There are two error terms that enter in the analysis: the reconstruction error due to the fact that the ambiguity function will only be determined on the bounded domain $\Omega := \bigcup_j \Omega_j$ and the propagation of the noise terms η_j . We will denote by \tilde{f} and \tilde{f}^η the reconstructions from F_j 's and F_j^η 's, respectively. The two error terms we need to bound are on the right-hand side (RHS) of

$$\|f - \tilde{f}^\eta\|_{L^p(\mathbb{R})} \leq \|f - \tilde{f}\|_{L^p(\mathbb{R})} + \|\tilde{f} - \tilde{f}^\eta\|_{L^p(\mathbb{R})},$$

where the first term on the RHS is the approximation error and the second is the propagation of data noise.

3.1. Stability of Algorithm 2.1. This subsection analyzes the stability of Algorithm 2.1.

3.1.1. Propagation of data noise. We start by estimating the second term, $\|\tilde{f} - \tilde{f}^\eta\|_{L^p(\mathbb{R})}$. For this, let A and A^η denote the functions obtained on $\Omega = \bigcup_{j=1}^N \Omega_j$ through the reconstruction formula (2.2) from F_j, F_j^η , respectively. That is,

$$A(x, y) = \frac{\sum_{j=1}^N \mathcal{F}(F_j)(y, -x)}{\sum_{j=1}^N \mathcal{A}\phi_j(x, y)}, \quad A^\eta(x, y) = \frac{\sum_{j=1}^N \mathcal{F}(F_j^\eta)(y, -x)}{\sum_{j=1}^N \mathcal{A}\phi_j(x, y)}, \quad (x, y) \in \Omega.$$

Since the reconstructions are only computed on Ω , we simply set A and A^η to zero on $\mathbb{R}^2 \setminus \Omega$. This does not affect the data noise propagation, but the fact that the ambiguity function will only

be recovered on Ω will enter in the reconstruction error term later. To this end, we introduce the mixed-norm $L^{p,1}$ space consisting of all functions U on \mathbb{R}^2 for which

$$\|U\|_{L^{p,1}(\mathbb{R}^2)} := \int_{\mathbb{R}} \left(\int_{\mathbb{R}} |U(x, y)|^p dx \right)^{1/p} dy < \infty.$$

We derive the following bounds on the propagation of data noise in the ambiguity functions.

LEMMA 3.1. *Let A, A^η be the reconstructions obtained by (2.2) from F_j, F_j^η , respectively, $j = 1, \dots, N$ and for some $\varepsilon > 0$, let Ω be chosen such that $\sum_{j=1}^N \mathcal{A}\phi_j(x, y) > \varepsilon$ for all $(x, y) \in \Omega$. Then,*

$$(3.1) \quad \|A - A^\eta\|_{L^{p,1}(\mathbb{R}^2)} \leq \frac{C_p}{\varepsilon} \left\| \sum_{j=1}^N \eta_j \right\|_{W^{1,1}(\mathbb{R}^2)},$$

where $C_p := \|\mathbb{1}_\Omega/\omega\|_{L^{p,1}(\mathbb{R}^2)}$, $\mathbb{1}_\Omega$ denotes the characteristic function on Ω and $\omega(x, y) := 1 + 2\pi i(x + y)$. Furthermore,

$$(3.2) \quad \|A(0, \cdot) - A^\eta(0, \cdot)\|_{L^1(\mathbb{R})} \leq \frac{C_{\mathbb{R}, \Omega}}{\varepsilon} \cdot \left\| \sum_{j=1}^N \eta_j \right\|_{L^1(\mathbb{R}^2)},$$

where $C_{\mathbb{R}, \Omega} := |\Omega_x|$ where $\Omega_x = \{x \in \mathbb{R} : (x, 0) \in \Omega\} \subset \mathbb{R}$.

Proof. Formula (2.2) gives

$$\|A - A^\eta\|_{L^{p,1}(\mathbb{R}^2)} = \left\| \mathbb{1}_\Omega \frac{\sum_{j=1}^N T\mathcal{F}(F_j - F_j^\eta)}{\sum_{j=1}^N \mathcal{A}\phi_j} \right\|_{L^{p,1}(\mathbb{R}^2)} \leq \frac{C_p}{\varepsilon} \left\| \omega T \sum_{j=1}^N \mathcal{F}(F_j - F_j^\eta) \right\|_{L^\infty(\mathbb{R}^2)},$$

where $T(\cdot)(x, y) = (\cdot)(y, -x)$. This can be further estimated by

$$\begin{aligned} \|A - A^\eta\|_{L^{p,1}(\mathbb{R}^2)} &\leq \frac{C_p}{\varepsilon} \left\| \tilde{\omega} \mathcal{F} \left(\sum_{j=1}^N \eta_j \right) \right\|_{L^\infty(\mathbb{R}^2)} \\ &\leq \frac{C_p}{\varepsilon} \left\| \mathcal{F} \left(\sum_{j=1}^N \left(\eta_j - \frac{\partial}{\partial x} \eta_j + \frac{\partial}{\partial y} \eta_j \right) \right) \right\|_{L^\infty(\mathbb{R}^2)} \leq \frac{C_p}{\varepsilon} \left\| \sum_{j=1}^N \eta_j \right\|_{W^{1,1}(\mathbb{R}^2)}, \end{aligned}$$

with $\tilde{\omega} := T\omega = (1 + 2\pi i(y - x))$ and by employing the Hausdorff-Young inequality in the last

step. Finally, (3.2) can be obtained as

$$\begin{aligned}
\|A(0, \cdot) - A^\eta(0, \cdot)\|_{L^1(\mathbb{R})} &\leq \left\| \frac{\sum_{j=1}^N T\mathcal{F}(F_j - F_j^\eta)(0, \cdot)}{\sum_{j=1}^N \mathcal{A}\phi_j} \right\|_{L^1(\Omega \cap (\{0\} \times \mathbb{R}))}, \\
&\leq \frac{1}{\varepsilon} \left\| \sum_{j=1}^N \mathcal{F}\eta_j(\cdot, 0) \right\|_{L^1(\Omega_x)}, \\
&\leq \frac{C_{\mathbb{R}, \Omega}}{\varepsilon} \left\| \sum_{j=1}^N \mathcal{F}\eta_j(\cdot, 0) \right\|_{L^\infty(\mathbb{R})}, \\
&\leq \frac{C_{\mathbb{R}, \Omega}}{\varepsilon} \left\| \mathcal{F}\left(\sum_{j=1}^N \eta_j\right) \right\|_{L^\infty(\mathbb{R}^2)}, \\
&\leq \frac{C_{\mathbb{R}, \Omega}}{\varepsilon} \cdot \left\| \sum_{j=1}^N \eta_j \right\|_{L^1(\mathbb{R}^2)}, \quad \square
\end{aligned}$$

where the last inequality is an application of the Hausdorff-Young inequality. To bound the propagation of data noise in the reconstructions \tilde{f} and \tilde{f}^η , we first define

$$\begin{aligned}
\tilde{u}_c(x) &:= \int_{\mathbb{R}} A(x, y) e^{2\pi i(x/2+c)y} dy, \\
\tilde{u}_c^\eta(x) &:= \int_{\mathbb{R}} A^\eta(x, y) e^{2\pi i(x/2+c)y} dy,
\end{aligned}$$

for $c \in \mathbb{R}$ and note that their difference can be straightforwardly bounded by

$$\begin{aligned}
\|\tilde{u}_c - \tilde{u}_c^\eta\|_{L^p(\mathbb{R})} &\leq \left(\int_{\mathbb{R}} \left| \int_{\mathbb{R}} (A(x, y) - A^\eta(x, y)) e^{2\pi i(x/2+c)y} dy \right|^p dx \right)^{1/p}, \\
&\leq \left(\int_{\mathbb{R}} \left| \int_{\mathbb{R}} |A(x, y) - A^\eta(x, y)| dy \right|^p dx \right)^{1/p}, \\
(3.3) \quad &\leq \int_{\mathbb{R}} \left(\int_{\mathbb{R}} |A(x, y) - A^\eta(x, y)|^p dx \right)^{1/p} dy = \|A - A^\eta\|_{L^{p,1}(\mathbb{R}^2)},
\end{aligned}$$

where the last inequality is an application of Minkowski's integral inequality.

For reconstructing from $\tilde{u}_c, \tilde{u}_c^\eta$, it is necessary to fix a point $c \in \mathbb{R}$ such that $|\tilde{u}_c(0)| \neq 0$ and $|\tilde{u}_c^\eta(0)| \neq 0$. Without loss of generality and for simpler notation, suppose that one can choose $c = 0$ and denote $\tilde{u}(x) := \tilde{u}_0(x)$, $\tilde{u}^\eta(x) := \tilde{u}_0^\eta(x)$. Then, the reconstructions are obtained by taking

$$\begin{aligned}
\tilde{f}(x) &= \frac{1}{\sqrt{|\tilde{u}(0)|}} \tilde{u}(x), \\
\tilde{f}^\eta(x) &= \frac{1}{\sqrt{|\tilde{u}^\eta(0)|}} \tilde{u}^\eta(x),
\end{aligned}$$

which corresponds to setting the phase factor at $x = 0$ to be equal to 1, i.e., $\tilde{f}(0) = |\tilde{f}(0)|$ and $\tilde{f}^\eta(0) = |\tilde{f}^\eta(0)|$. Note that with the choice above, $|\tilde{f}(0)| = \sqrt{|\tilde{u}(0)|}$ and $|\tilde{f}^\eta(0)| = \sqrt{|\tilde{u}^\eta(0)|}$.

The propagation of data noise on the reconstructions \tilde{f} and \tilde{f}^η can be estimated as follows:

PROPOSITION 3.2. *Let $k := \sqrt{|\tilde{u}(0)|}$ and $k^\eta := \sqrt{|\tilde{u}^\eta(0)|}$. Then,*

$$(3.4) \quad \left\| \tilde{f} - \tilde{f}^\eta \right\|_{L^p(\mathbb{R})} \leq \left(\frac{\|A\|_{L^{p,1}(\mathbb{R}^2)}}{2(k k^\eta)^{3/2}} + \frac{1}{k^\eta} \right) \frac{\max(C_{\mathbb{R},\Omega}, C_p)}{\varepsilon} \left\| \sum_{j=1}^N \eta_j \right\|_{W^{1,1}(\mathbb{R}^2)}.$$

Proof. We have

$$\begin{aligned} \left\| \tilde{f} - \tilde{f}^\eta \right\|_{L^p(\mathbb{R})} &\leq \left\| \frac{1}{k} \cdot \tilde{u} - \frac{1}{k^\eta} \cdot \tilde{u} \right\|_{L^p(\mathbb{R})} + \left\| \frac{1}{k^\eta} \cdot \tilde{u} - \frac{1}{k^\eta} \cdot \tilde{u}^\eta \right\|_{L^p(\mathbb{R})}, \\ &\leq \left| \frac{1}{k} - \frac{1}{k^\eta} \right| \cdot \|\tilde{u}\|_{L^p(\mathbb{R})} + \frac{1}{k^\eta} \|\tilde{u} - \tilde{u}^\eta\|_{L^p(\mathbb{R})}, \\ &\leq \frac{1}{2(k k^\eta)^{3/2}} |(k^\eta)^2 - k^2| \cdot \|\tilde{u}\|_{L^p(\mathbb{R})} + \frac{1}{k^\eta} \|\tilde{u} - \tilde{u}^\eta\|_{L^p(\mathbb{R})}, \\ &\leq \frac{1}{2(k k^\eta)^{3/2}} |\tilde{u}^\eta(0) - \tilde{u}(0)| \cdot \|\tilde{u}\|_{L^p(\mathbb{R})} + \frac{1}{k^\eta} \|\tilde{u} - \tilde{u}^\eta\|_{L^p(\mathbb{R})}, \end{aligned}$$

where the arithmetic-geometric mean inequality is applied in the third line (since $k, k^\eta > 0$) and the reverse triangle inequality is used in the fourth line. Combining this with (3.3), we obtain

$$\left\| \tilde{f} - \tilde{f}^\eta \right\|_{L^p(\mathbb{R})} \leq \frac{1}{2(k k^\eta)^{3/2}} \|A(0, \cdot) - A^\eta(0, \cdot)\|_{L^1(\mathbb{R})} \cdot \|A\|_{L^{p,1}(\mathbb{R}^2)} + \frac{1}{k^\eta} \|A - A^\eta\|_{L^{p,1}(\mathbb{R}^2)}.$$

Further estimating the RHS employing (3.1) and (3.2) yields the desired bound. \square

3.1.2. Approximation error. The error bound in (3.4) becomes small as we increase ε . However, this comes at the cost of increasing $\|f - \tilde{f}\|$ since we only recover $\mathcal{A}f$ or its approximation on the bounded domain $\Omega = \bigcup_{j=1}^N \Omega_j$ decided by ε . The bound on the approximation error $\|f - \tilde{f}\|$ will depend on the quantities

$$(3.5) \quad \|\mathcal{A}f\|_{L^{p,1}(\mathbb{R}^2 \setminus \Omega)} := \|\mathbb{1}_{\mathbb{R}^2 \setminus \Omega} \mathcal{A}f\|_{L^{p,1}(\mathbb{R}^2)},$$

and

$$(3.6) \quad \|\mathcal{A}f(0, \cdot)\|_{L^1((\mathbb{R}^2 \setminus \Omega) \cap (\{0\} \times \mathbb{R}))}.$$

Note that $|\mathcal{A}f| = |V_f f|$, so (3.5) quantifies the decay of both f and its Fourier transform \hat{f} . Moreover, (3.6) gives the decay of $|\mathcal{F}(|f|^2)|$ since $|\mathcal{A}f(0, \cdot)| = |\mathcal{F}(|f|^2)|$.

We further note that since A and $\mathcal{A}f$ agree on Ω and A is identical to zero on $\mathbb{R}^2 \setminus \Omega$, we have

$$\|A - \mathcal{A}f\|_{L^{p,1}(\mathbb{R}^2)} = \|A - \mathcal{A}f\|_{L^{p,1}(\mathbb{R}^2 \setminus \Omega)} = \|\mathcal{A}f\|_{L^{p,1}(\mathbb{R}^2 \setminus \Omega)},$$

and, similar to (3.3),

$$\|u - \tilde{u}\|_{L^p(\mathbb{R})} \leq \|\mathcal{A}f - A\|_{L^{p,1}(\mathbb{R}^2)},$$

where $u(x) := \int_{\mathbb{R}} \mathcal{A}f(x, y) e^{\pi i x y} dy$. Note that $u(0) = |f(0)|^2 > 0$ and define $k^{\text{true}} := \sqrt{u(0)}$. As before, we take $k = \sqrt{|\tilde{u}(0)|}$ and set the phase factors of f and \tilde{f} to 1 at $x = 0$. With this, we obtain the following lemma.

LEMMA 3.3. *Let f be the true solution and let \tilde{f} be the reconstruction from F_1, \dots, F_N by formula (2.2). Then,*

$$(3.7) \quad \left\| f - \tilde{f} \right\|_{L^p(\mathbb{R})} \leq \frac{1}{k^{\text{true}}} \|\mathcal{A}f\|_{L^{p,1}(\mathbb{R}^2 \setminus \Omega)} + \frac{\|A\|_{L^{p,1}(\mathbb{R}^2)}}{2(k^{\text{true}} k)^{3/2}} \|\mathcal{A}f(0, \cdot)\|_{L^1((\mathbb{R}^2 \setminus \Omega) \cap (\{0\} \times \mathbb{R}))}.$$

Proof. We first use the triangle inequality and split the approximation error into two terms. Recalling that

$$\tilde{u}(x) = \int_{\mathbb{R}} A(x, y) e^{\pi i x y} dy \quad \text{and} \quad \tilde{f}(x) = \tilde{u}(x)/k,$$

we obtain

$$\begin{aligned} \|f - \tilde{f}\|_{L^p(\mathbb{R})} &\leq \left\| f - \frac{\tilde{u}}{k^{\text{true}}} \right\|_{L^p(\mathbb{R})} + \left\| \frac{\tilde{u}}{k^{\text{true}}} - \tilde{f} \right\|_{L^p(\mathbb{R})} \\ &= \left\| \frac{u}{k^{\text{true}}} - \frac{\tilde{u}}{k^{\text{true}}} \right\|_{L^p(\mathbb{R})} + \left\| \frac{\tilde{u}}{k^{\text{true}}} - \tilde{f} \right\|_{L^p(\mathbb{R})} \\ &\leq \frac{1}{k^{\text{true}}} \|\mathcal{A}f\|_{L^{p,1}(\mathbb{R}^2 \setminus \Omega)} + \left| \frac{1}{k^{\text{true}}} - \frac{1}{k} \right| \cdot \|\tilde{u}\|_{L^p(\mathbb{R})} \\ &\leq \frac{1}{k^{\text{true}}} \|\mathcal{A}f\|_{L^{p,1}(\mathbb{R}^2 \setminus \Omega)} + \left| \frac{1}{k^{\text{true}}} - \frac{1}{k} \right| \cdot \|A\|_{L^{p,1}(\mathbb{R}^2)}. \end{aligned}$$

Similar to the derivations of the noise propagation term, we can further bound this by

$$\begin{aligned} \|f - \tilde{f}\|_{L^p(\mathbb{R})} &\leq \frac{1}{k^{\text{true}}} \|\mathcal{A}f\|_{L^{p,1}(\mathbb{R}^2 \setminus \Omega)} + \frac{1}{2(k^{\text{true}} k)^{3/2}} |u(0) - \tilde{u}(0)| \cdot \|A\|_{L^{p,1}(\mathbb{R}^2)} \\ &\leq \frac{1}{k^{\text{true}}} \|\mathcal{A}f\|_{L^{p,1}(\mathbb{R}^2 \setminus \Omega)} + \frac{1}{2(k^{\text{true}} k)^{3/2}} \|\mathcal{A}f(0, \cdot) - A(0, \cdot)\|_{L^1(\mathbb{R})} \cdot \|A\|_{L^{p,1}(\mathbb{R}^2)} \\ &\leq \frac{1}{k^{\text{true}}} \|\mathcal{A}f\|_{L^{p,1}(\mathbb{R}^2 \setminus \Omega)} + \frac{1}{2(k^{\text{true}} k)^{3/2}} \|\mathcal{A}f(0, \cdot)\|_{L^1((\mathbb{R}^2 \setminus \Omega) \cap (\{0\} \times \mathbb{R}))} \cdot \|A\|_{L^{p,1}(\mathbb{R}^2)}. \quad \square \end{aligned}$$

3.1.3. Total error. We are now in a position to combine the estimates (3.4) and (3.7) on propagation of data noise and approximation error to a total error estimate.

PROPOSITION 3.4. *For some constant $C > 0$ depending on $\|A\|_{L^{p,1}(\mathbb{R}^2)}$, k , k^η , k^{true} , $C_{\mathbb{R}, \Omega}$ and C_p , we have*

$$\begin{aligned} \|f - \tilde{f}^\eta\|_{L^p(\mathbb{R})} &\leq \frac{1}{k^{\text{true}}} \|\mathcal{A}f\|_{L^{p,1}(\mathbb{R}^2 \setminus \Omega)} + \frac{1}{2(k^{\text{true}} k)^{3/2}} \|\mathcal{A}f(0, \cdot)\|_{L^1((\mathbb{R}^2 \setminus \Omega) \cap (\{0\} \times \mathbb{R}))} \cdot \|A\|_{L^{p,1}(\mathbb{R}^2)} \\ &\quad + \left(\frac{1}{2(k k^\eta)^{3/2}} \cdot \|A\|_{L^{p,1}(\mathbb{R}^2)} + \frac{1}{k^\eta} \right) \cdot \frac{1}{\varepsilon} \max(C_{\mathbb{R}, \Omega}, C_p) \left\| \sum_{j=1}^N \eta_j \right\|_{W^{1,1}(\mathbb{R}^2)} \\ (3.8) \quad &\leq C \cdot \left(\|\mathcal{A}f\|_{L^{p,1}(\mathbb{R}^2 \setminus \Omega)} + \|\mathcal{A}f(0, \cdot)\|_{L^1((\mathbb{R}^2 \setminus \Omega) \cap (\{0\} \times \mathbb{R}))} + \frac{1}{\varepsilon} \left\| \sum_{j=1}^N \eta_j \right\|_{W^{1,1}(\mathbb{R}^2)} \right). \end{aligned}$$

Remark 3.5. There are three terms on the RHS of (3.8). The first two terms depend on $\Omega = \cup_{j=1}^N \Omega_j$, which is determined by the choice of ε . As ε increases, so do the first two terms. Conversely, the last term is inversely proportional to ε . Therefore, one must balance these terms when selecting an appropriate ε .

Now, consider a fixed ε . If we only use a single window function, i.e., $N = 1$, then the set Ω can be significantly smaller compared to the case with multiple windows; see Figures 1 and 2 for illustrations. This again sheds lights on the fact that we achieve better stability by using more windows. In this way, we can significantly reduce the magnitude of the first two terms in (3.8) while keeping the last term constant.

3.2. Stability of Algorithm 2.2. In Algorithm 2.2, the reconstruction is done separately on each Ω_j , using F_j, F_j^η for computing A, A^η , respectively. Again, A and A^η will be set to zero outside of Ω and we obtain the following error bound for the data noise propagation:

LEMMA 3.6. *Let A, A^η be the reconstructions obtained from F_j, F_j^η , respectively, $j = 1, \dots, N$, and for some $\varepsilon > 0$, let Ω_j be chosen such that $|\mathcal{A}h_{n_j}(x, y)| > \varepsilon$ for all $(x, y) \in \Omega_j$ for all $j \in \{1, \dots, N\}$. Then,*

$$\begin{aligned} \|A - A^\eta\|_{L^{p,1}(\mathbb{R}^2)} &\leq \frac{C_p}{\varepsilon} \max_{j=1, \dots, N} \|\eta_j\|_{W^{1,1}(\mathbb{R}^2)}, \\ \|A(0, \cdot) - A^\eta(0, \cdot)\|_{L^1(\mathbb{R})} &\leq \frac{C_{\mathbb{R}, \Omega}}{\varepsilon} \cdot \max_{j=1, \dots, N} \|\eta_j\|_{L^1(\mathbb{R}^2)}. \end{aligned}$$

Proof. By the reconstruction formula,

$$\|A - A^\eta\|_{L^{p,1}(\mathbb{R}^2)} \leq \sum_{j=1}^N \left\| \mathbf{1}_{\Omega_j} \frac{T\mathcal{F}(F_j - F_j^\eta)}{\mathcal{A}h_{n_j}} \right\|_{L^{p,1}(\mathbb{R}^2)} \leq \sum_{j=1}^N C_{j,p} \cdot \left\| \mathbf{1}_{\Omega_j} \omega \frac{T\mathcal{F}(F_j - F_j^\eta)}{\mathcal{A}h_{n_j}} \right\|_{L^\infty(\mathbb{R}^2)},$$

where $C_{j,p} := \|\mathbf{1}_{\Omega_j}/\omega\|_{L^{p,1}(\mathbb{R}^2)} < \infty$ and instead of (3.1), we now have the similar bound

$$\begin{aligned} \|A - A^\eta\|_{L^{p,1}(\mathbb{R}^2)} &\leq \sum_{j=1}^N \frac{C_{j,p}}{\inf_{\Omega_j} |\mathcal{A}h_{n_j}|} \cdot \|\tilde{\omega} \mathcal{F}\eta_j\|_{L^\infty(\mathbb{R}^2)} \\ &\leq \frac{1}{\varepsilon} \sum_{j=1}^N C_{j,p} \cdot \left\| \mathcal{F} \left(\eta_j - \frac{\partial}{\partial x} \eta_j + \frac{\partial}{\partial y} \eta_j \right) \right\|_{L^\infty(\mathbb{R}^2)} \\ &\leq \frac{1}{\varepsilon} \sum_{j=1}^N C_{j,p} \cdot \|\eta_j\|_{W^{1,1}(\mathbb{R}^2)} \leq \frac{C_p}{\varepsilon} \max_{j=1, \dots, N} \|\eta_j\|_{W^{1,1}(\mathbb{R}^2)}, \end{aligned}$$

where we have used $\sum_{j=1}^N C_{j,p} = C_p$ since $\Omega_1, \dots, \Omega_N$ are pairwise disjoint and the Hausdorff-Young inequality. Similar to (3.2), we can further derive

$$\begin{aligned} \|A(0, \cdot) - A^\eta(0, \cdot)\|_{L^1(\mathbb{R})} &\leq \sum_{j=1}^N \left\| \frac{T\mathcal{F}(F_j - F_j^\eta)}{\mathcal{A}h_{n_j}}(0, \cdot) \right\|_{L^1(\Omega_j \cap (\{0\} \times \mathbb{R}))} \\ &\leq \frac{1}{\varepsilon} \sum_{j=1}^N \|\mathcal{F}\eta_j(\cdot, 0)\|_{L^1(\Omega_{j,x})} \\ &\leq \frac{1}{\varepsilon} \sum_{j=1}^N \|\mathcal{F}\eta_j(\cdot, 0)\|_{L^\infty(\mathbb{R})} \cdot |\Omega_{j,x}| \\ &\leq \frac{1}{\varepsilon} \sum_{j=1}^N \|\eta_j\|_{L^1(\mathbb{R}^2)} \cdot |\Omega_{j,x}| \\ &\leq \frac{C_{\mathbb{R}, \Omega}}{\varepsilon} \cdot \max_{j=1, \dots, N} \|\eta_j\|_{L^1(\mathbb{R}^2)}, \end{aligned} \quad \square$$

where $\Omega_{j,x} = \{x \in \mathbb{R} : (x, 0) \in \Omega_j\} \subset \mathbb{R}$.

With this, the propagation of data noise can be estimated by

$$\|\tilde{f} - \tilde{f}^\eta\|_{L^p(\mathbb{R})} \leq \left(\frac{1}{2(kk^\eta)^{3/2}} \cdot \|A\|_{L^{p,1}(\mathbb{R}^2)} + \frac{1}{k^\eta} \right) \cdot \frac{1}{\varepsilon} \max(C_{\mathbb{R}, \Omega}, C_p) \max_{j=1, \dots, N} \|\eta_j\|_{W^{1,1}(\mathbb{R}^2)}.$$

The approximation error is the same as in the previous case (cf. (3.7)), so that the total error can be bounded by

$$\begin{aligned}
\|f - \tilde{f}^\eta\|_{L^p(\mathbb{R})} &\leq \frac{1}{k^{\text{true}}} \|\mathcal{A}f\|_{L^{p,1}(\mathbb{R}^2 \setminus \Omega)} + \frac{1}{2(k^{\text{true}} k)^{3/2}} \|\mathcal{A}f(0, \cdot)\|_{L^1((\mathbb{R}^2 \setminus \Omega) \cap (\{0\} \times \mathbb{R}))} \cdot \|A\|_{L^{p,1}(\mathbb{R}^2)} \\
&\quad + \left(\frac{1}{2(k k^\eta)^{3/2}} \cdot \|A\|_{L^{p,1}(\mathbb{R}^2)} + \frac{1}{k^\eta} \right) \cdot \frac{1}{\varepsilon} \max(C_{\mathbb{R}, \Omega}, C_p) \max_{j=1, \dots, N} \|\eta_j\|_{W^{1,1}(\mathbb{R}^2)} \\
(3.9) \quad &\leq C \cdot \left(\|\mathcal{A}f\|_{L^{p,1}(\mathbb{R}^2 \setminus \Omega)} + \|\mathcal{A}f(0, \cdot)\|_{L^1((\mathbb{R}^2 \setminus \Omega) \cap (\{0\} \times \mathbb{R}))} + \frac{1}{\varepsilon} \max_{j=1, \dots, N} \|\eta_j\|_{W^{1,1}(\mathbb{R}^2)} \right),
\end{aligned}$$

for some constant $C > 0$ depending on $\|A\|_{L^{p,1}(\mathbb{R}^2)}$, k , k^η , k^{true} , $C_{\mathbb{R}, \Omega}$ and C_p .

The third term on the RHS is the only difference between (3.8) and (3.9). The former depends on the maximum noise power, while the latter involves the sum of the noise for different window functions. Their differences result from the distinctions between Algorithms 2.1 and 2.2 regarding how the multi-window measurements are utilized in the STFT phase retrieval.

4. Numerical examples. In this section, we present a few 1D phase retrieval examples using the explicit formula (1.2)-(1.4), given the phaseless measurement $|V_g f|$ and the ambiguity function $\mathcal{A}g$ of the window function g or $V_g g$.

4.1. Discretization. Recall the continuous STFT transform given in Equation (1.1). If we know the function f is compactly supported on a finite interval of \mathbb{R} , e.g., $[-T, T]$ for some $T > 0$, then we can perform the integration on $[-T, T]$:

$$(4.1) \quad V_g f(x, y) := \int_{-T}^T f(t) \overline{g(t-x)} e^{-2\pi i t y} dt.$$

Without loss of generality, we only consider periodic window functions $g(t)$ on $[-T, T]$, i.e., $g(-t) = g(2T - t)$. All Hermite and Gauss windows used in the numerical examples are periodized.

For the numerical integration, consider an equidistant discretization in time such that $f_l := f(x_l)$, $x_l = -T + l\Delta t$, $0 \leq l \leq L-1$ and $L = 2T/\Delta t$. We compute the STFT at K equidistant time-domain shifts $x_0, \dots, x_k, \dots, x_{K-1}$, based on the uniform spacing $a\Delta t$ with $a \in \mathbb{N}^+$ and $K = L/a$. Similarly, we discretize the frequency domain interval $[-\frac{1}{2\Delta t}, \frac{1}{2\Delta t}]$ uniformly by taking M points, i.e., $y_m = \frac{1}{\Delta t} (-\frac{1}{2} + \frac{m}{M})$ for $0 \leq m < M$. Note that $1/(2\Delta t)$ is the Nyquist frequency. Using the left Riemann sum, (4.1) can be approximated by

$$(4.2) \quad c_{(m,k)} = \Delta t \sum_{l=0}^{L-1} f_l \overline{g_{l-ka+L/2}} e^{-2\pi i (-T+l\Delta t) \frac{1}{\Delta t} (-\frac{1}{2} + \frac{m}{M})},$$

where $m = 0, \dots, M-1$, and $k = 0, \dots, K-1$, with

$$c_{(m,k)} \approx V_g f \left(-T + ka\Delta t, \frac{1}{\Delta t} \left(-\frac{1}{2} + \frac{m}{M} \right) \right)$$

being the $(m+1, k+1)$ -th entry of the coefficient matrix c . The index $l - ka + L/2$ in (4.2) is computed modulo L since we assume that the window function g is periodic. That is,

$$g_{-s} = g(-T - s\Delta t) = g(T - s\Delta t) = g_{(2T-s\Delta t)/\Delta t} = g_{L-s}, \quad \forall s = 0, \dots, L-1.$$

There are many fast ways of implementing (4.2); see the toolbox [23] for an example. One should note that if $\Delta t = 1$, (4.2) reduces to the so-called Discrete Short-Time Fourier Transform (Discrete STFT).

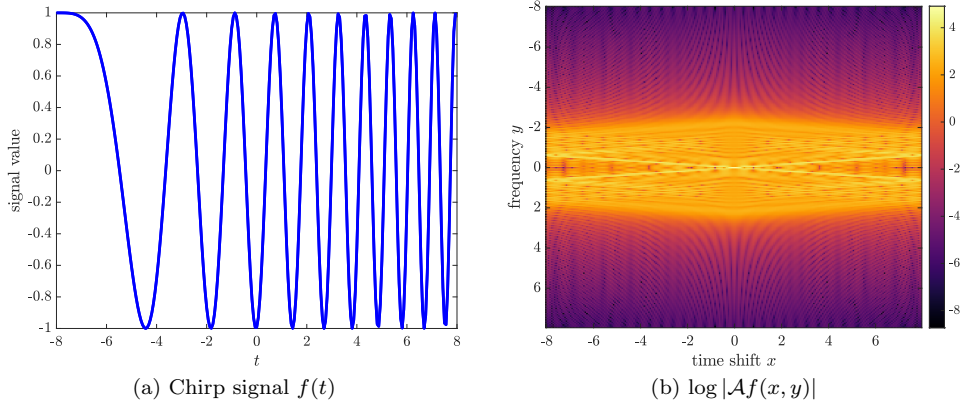


Fig. 3: (a) The ground truth chirp signal $f(t)$; (b) The absolute value of the ambiguity function of f plotted in the log scale.

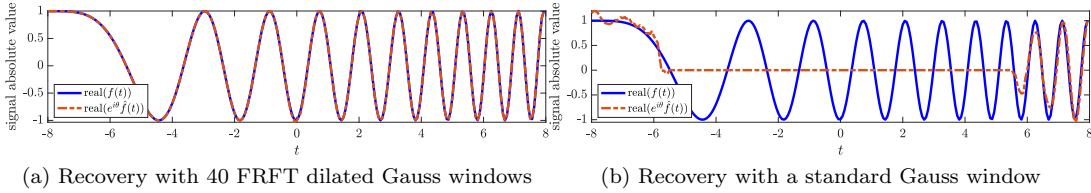


Fig. 4: (a) Recovery using 40 fractional Fourier transform of the dilated Gauss windows at various angles; (b) Recovery using a single standard Gauss window. The ground truth is plotted in blue.

Since the output of our proposed algorithms recovers the original signal up to a global phase, we define the following misfit function $d(\cdot, \cdot)$ that measures the relative error between two signals f_1 and f_2 up to a global phase factor:

$$(4.3) \quad d(f_1, f_2) = \min_{\theta \in [0, 2\pi)} \frac{\|f_1 - e^{i\theta} f_2\|_{\ell^2}}{\|f_1\|_{\ell^2}}.$$

The angle θ^* that minimizes (4.3) is also the missing global phase angle.

4.2. Synthetic examples. In this subsection, we will present two STFT phase retrieval examples using the proposed multi-window Algorithms 2.1 and 2.2.

4.2.1. Chirp signal recovery. As our first inversion example, we consider the chirp signal shown in Figure 3a. As illustrated in Figure 3b, its ambiguity function has extensive support in the time-frequency domain, making it challenging to reconstruct using a single window of the standard Gauss function whose ambiguity function has a very small essential support as seen in Figure 1a. We set $\varepsilon = 10^{-3}$ as a cutoff value, as used in Algorithms 2.1 and 2.2 to prevent the instability from dividing the phaseless measurements by a small value.

We first use 40 fractionally transformed dilated Gaussian windows to perform the reconstruction following Algorithm 2.1, i.e., $\mathcal{F}_{\alpha_j} \varphi^a$ with $a = 15$ and $\alpha_j = (j - 1)\pi/40$, $j = 1, \dots, 40$. The relative error based on formula (4.3) between the ground truth and the reconstructed signal is 0.0084. We also use the standard Gauss function φ^1 as a single window function for comparison.

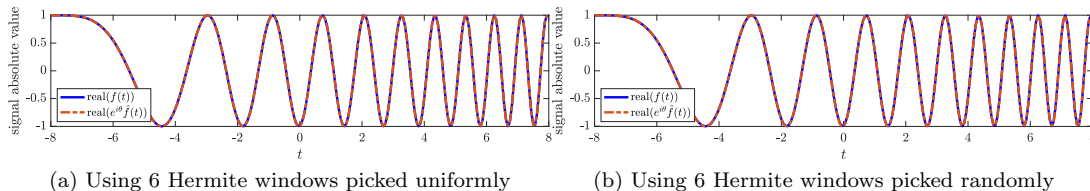


Fig. 5: (a) Recovery using 6 Hermite windows of h_n where $n = 0, 10, 20, 30, 40, 50$; (b) Recovery using 6 Hermite windows of h_n with the index n randomly selected between 0 and 50, resulting in a set of indices $\{17, 24, 29, 30, 31, 49\}$. The ground truth is plotted in blue.

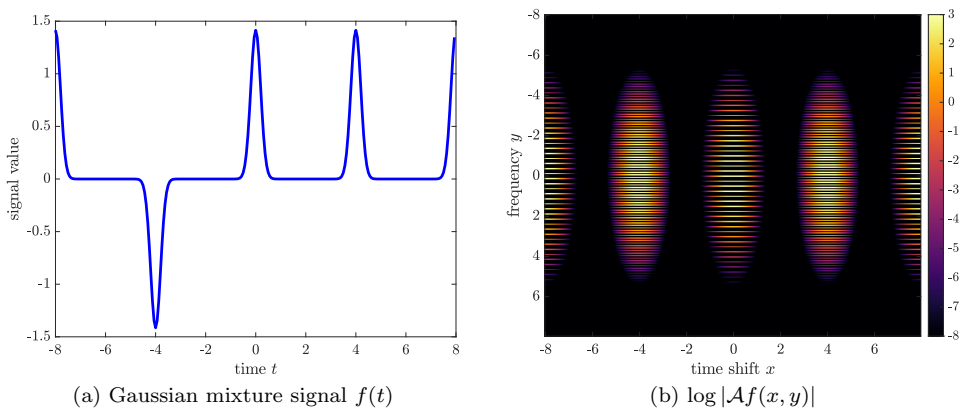


Fig. 6: Multi-modal function example: (a) The ground truth $f(t)$; (b) The absolute value of the ambiguity function of f plotted in the log scale.

The relative error is 0.7928. After finding the global phase factor, we plot the reconstructions under different measuring window schemes in Figure 4. More measuring windows yield a much more extensive joint coverage of the time-frequency domain, resulting in better signal reconstruction.

Next, we use multiple Hermite windows to perform the recovery. Consider 6 Hermite function h_n with $n \in \{0, 10, 20, 30, 40, 50\}$. We then follow Algorithm 2.2 to perform the inversion. The misfit between the reconstructed signal and the ground truth measured by (4.3) is 0.0025. On the other hand, we want to test the idea of randomly choosing window functions. We draw 6 windows uniformly from the zeroth to the fiftieth degree Hermite functions, and use them to generate the phaseless data and perform the STFT phase retrieval following Algorithm 2.2. We repeat this procedure 100 times to study the performance of this inversion algorithm. The mean relative error measured by (4.3) between the ground truth and the reconstructed signal is 0.0298. In particular, 90% of the randomly picked window sets yield signal reconstructions with relative error less than 0.0320. We also plot the reconstruction results from the uniformly chosen windows and one realization of the randomly selected windows in Figure 5.

4.2.2. Recovery of a multi-modal function with noisy measurements. We consider a multi-modal function plotted in Figure 6a, a linear combination of time-shifts of φ^4 , the dilated Gauss function. The absolute value of its ambiguity function in log scale is shown in Figure 6b. This signal is known to cause stability issues in STFT phase retrieval [2, Sec. 6]. The measurement is contaminated by a multiplicative noise following the normal distribution $\mathcal{N}(1, 0.05^2)$; see Figure 7

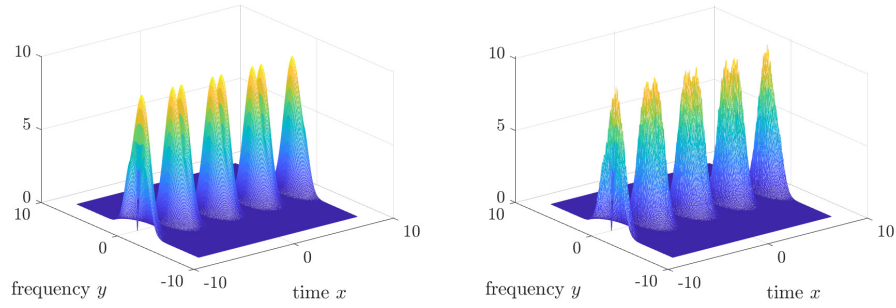
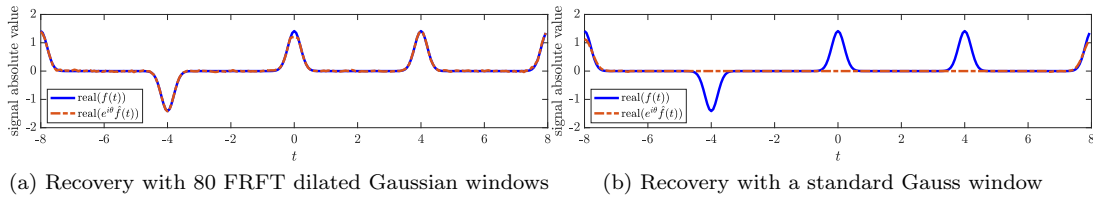


Fig. 7: Multi-modal function example: the noise-free measurement of $|V_g f|$ for $g = \varphi^1$ (left) and the noisy data used in phase retrieval (right).



(a) Recovery with 80 FRFT dilated Gaussian windows (b) Recovery with a standard Gauss window

Fig. 8: Multi-modal function example: (a) Recovery using 80 fractional Fourier transforms of the dilated Gauss window at various angles; (b) Recovery using a single standard Gauss window. The ground truth is plotted in blue.

for an example.

We consider the cutoff value $\varepsilon = 0.5$ to define the essential support of the ambiguity function in [Algorithms 2.1](#) and [2.2](#). Since ε is large, we need to measure windows whose ambiguity functions have broader support in the time-frequency domain to perform the inversion. We first use fractionally Fourier-transformed versions of the dilated Gauss function φ^{50} as the measuring windows. Since the essential support of these ambiguity functions is thin and long, we need to take more windows at different angles to achieve broad coverage of the joint essential support in the time-frequency domain: we use 80 angles with $\alpha_j = (j - 1)\pi/40$, $j = 1, \dots, 80$. The recovery is shown in [Figure 8](#), compared with the case using the standard Gauss as the measuring function. As seen in [Figure 6b](#), the ambiguity function of the ground truth has almost disjoint support in the time-frequency domain. It thus cannot be stably recovered by a single Gauss window, as shown in [Figure 8b](#), while the multiple fractional window strategy provides a stable recovery even under noisy measurement; see [Figure 8a](#).

Next, we also use Hermite functions as the measuring windows. In [Figure 9a](#), we use h_{50} and h_{100} , the Hermite functions of degree 50 and 100, to perform STFT phase retrieval following [Algorithm 2.2](#). We recover most features of the multi-modal function with minimal impact from the measurement noise illustrated in [Figure 7](#). We also compare the inversion result using the single window h_{100} in [Figure 9b](#). Although $\mathcal{A}h_{100}$ has extensive overall coverage in the time-frequency domain, it also has 100 circular rings that are excluded since their absolute value is below the cutoff value ε . As a result, the reconstruction is affected by those missing data. The ambiguity function $\mathcal{A}h_{50}$ of the additional window h_{50} makes up most of those “missing” rings, so the reconstruction is much better.

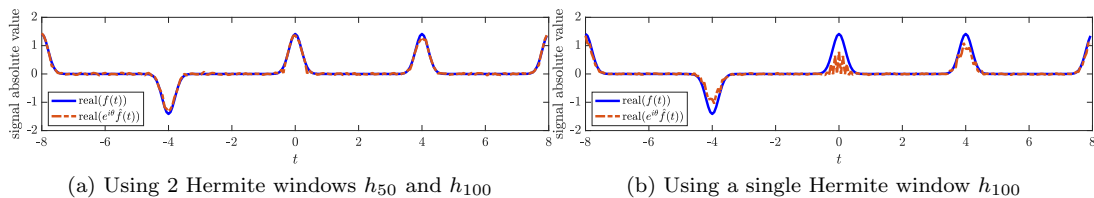


Fig. 9: Multi-modal function example: (a) Recovery using two Hermite windows h_n where $n = 50, 100$, and the relative error is 0.0899; (b) Recovery using the single Hermite window h_{100} , and the relative error is 0.4403 measured by (4.3). The true signal is plotted in blue.

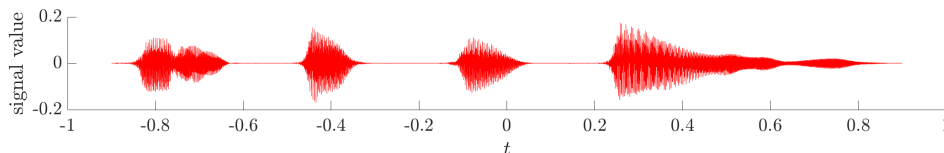


Fig. 10: The reference audio signal (in full length).

The large cutoff value ε mitigates the impact of noise, while using multiple windows improves the coverage in the time-frequency domain of the joint essential support of the corresponding ambiguity functions. This is evident from both using multiple fractionally Fourier-transformed dilated Gauss functions and Hermite functions of various degrees.

4.3. Audio data example. Our final numerical example involves recovering a piece of an audio signal, as illustrated in Figure 10. This audio signal is significantly more complex than the earlier synthetic examples, yet the proposed multi-window strategy proves effective for the phase retrieval task.

We utilize Algorithm 2.2 with different sets of Hermite functions. The resulting audio files, saved as `.wav` files, are provided in the supplementary materials. To visualize the reconstruction performance, we plot a small segment of both the true and recovered signals. The true audio signal is shown in Figure 11a, while the recovered segments are displayed in Figures 11b, 11c, and 11d, corresponding to the use of the window function h_1 , the pair $\{h_1, h_2\}$, and the set $\{h_0, h_5, h_{10}, h_{15}, h_{20}\}$, respectively. As more windows are incorporated according to Algorithm 2.2, the quality of the audio signal recovery progressively improves.

5. Conclusions. In this paper, we introduce two multi-window strategies to improve the stability of STFT phase retrieval. The first approach uses fractional Fourier transforms of dilated Gaussian functions at various angles, while the second employs Hermite functions of different degrees as window functions. As proven in our theory, both methods effectively broaden the coverage of the ambiguity function in the time-frequency domain, significantly mitigating the instability issues associated with traditional single-window approaches. Our numerical experiments demonstrate that these multi-window strategies greatly improve the stability and accuracy of phase retrieval, even for complex audio signals. These results suggest that combining measurements from carefully chosen windows can lead to more robust and reliable signal reconstruction through our simple and direct Algorithms 2.1 and 2.2.

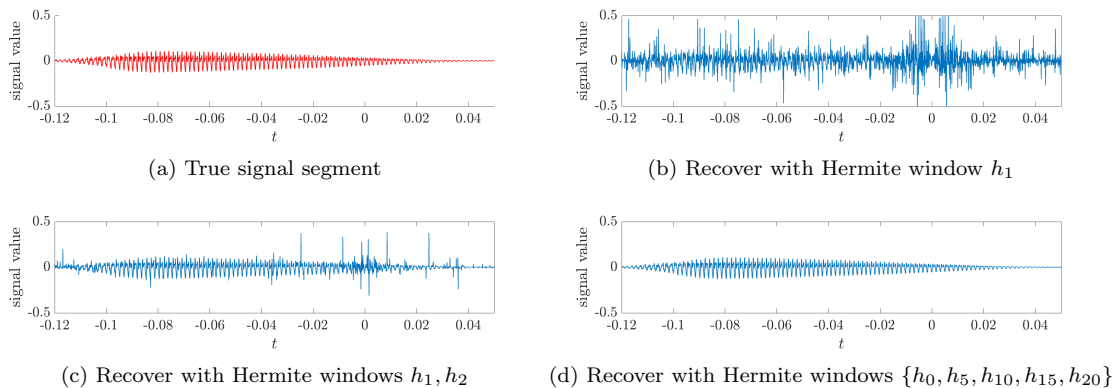


Fig. 11: Audio data STFT phase retrieval example: (a) The true signal segment; (b) Recovery using single Hermite window h_1 ; (c) Recovery using two Hermite windows h_1 and h_2 ; (d) Recovery using five Hermite windows $\{h_0, h_5, h_{10}, h_{15}, h_{20}\}$.

- [1] L. D. ABREU AND H. G. FEICHTINGER, *Function spaces of polyanalytic functions*, Harmonic and complex analysis and its applications, (2014), pp. 1–38.
- [2] R. ALAIFARI, *Ill-posed problems: From linear to nonlinear and beyond*, Harmonic and Applied Analysis: From Radon Transforms to Machine Learning, (2021), pp. 101–148.
- [3] R. ALAIFARI, I. DAUBECHIES, P. GROHS, AND R. YIN, *Stable phase retrieval in infinite dimensions*, Foundations of Computational Mathematics, 19 (2019), pp. 869–900.
- [4] R. ALAIFARI AND P. GROHS, *Gabor phase retrieval is severely ill-posed*, Applied and Computational Harmonic Analysis, 50 (2021), pp. 401–419.
- [5] R. ALAIFARI AND M. WELLERSHOFF, *Uniqueness of STFT phase retrieval for bandlimited functions*, Applied and Computational Harmonic Analysis, 50 (2021), pp. 34–48.
- [6] L. B. ALMEIDA, *The fractional Fourier transform and time-frequency representations*, IEEE Transactions on signal processing, 42 (1994), pp. 3084–3091.
- [7] H. H. BAUSCHKE, P. L. COMBETTES, AND D. R. LUKE, *Finding best approximation pairs relative to two closed convex sets in Hilbert spaces*, Journal of Approximation theory, 127 (2004), pp. 178–192.
- [8] E. J. CANDÈS, X. LI, AND M. SOLTANOLKOTABI, *Phase retrieval from coded diffraction patterns*, Applied and Computational Harmonic Analysis, 39 (2015), pp. 277–299.
- [9] E. J. CANDÈS, T. STROHMER, AND V. VORONINSKI, *Phaselift: Exact and stable signal recovery from magnitude measurements via convex programming*, Communications on Pure and Applied Mathematics, 66 (2013), pp. 1241–1274.
- [10] P. CHEN AND A. FANNJIANG, *Fourier phase retrieval with a single mask by Douglas–Rachford algorithms*, Applied and computational harmonic analysis, 44 (2018), pp. 665–699.
- [11] J. DOUGLAS AND H. H. RACHFORD, *On the numerical solution of heat conduction problems in two and three space variables*, Transactions of the American mathematical Society, 82 (1956), pp. 421–439.
- [12] A. FANNJIANG AND T. STROHMER, *The numerics of phase retrieval*, Acta Numerica, 29 (2020), pp. 125–228.
- [13] A. FANNJIANG AND Z. ZHANG, *Fixed Point Analysis of Douglas–Rachford Splitting for Ptychography and Phase Retrieval*, SIAM Journal on Imaging Sciences, 13 (2020), pp. 609–650.
- [14] J. R. FIENUP, *Phase retrieval algorithms: a comparison*, Applied optics, 21 (1982), pp. 2758–2769.
- [15] R. GERCHBERG AND W. SAXTON, *A practical algorithm for the determination of phase from image and diffraction plane pictures*, SPIE milestone series MS, 94 (1994), pp. 646–646.
- [16] K. GRÖCHENIG, *Foundations of time-frequency analysis*, Springer Science & Business Media, 2001.
- [17] K. GRÖCHENIG, P. JAMING, AND E. MALINNIKOVA, *Zeros of the Wigner distribution and the short-time Fourier transform*, Revista Matemática Complutense, 33 (2020), pp. 723–744.
- [18] P. GROHS AND M. RATHMAIR, *Stable Gabor phase retrieval and spectral clustering*, Communications on Pure and Applied Mathematics, 72 (2019), pp. 981–1043.
- [19] P. JAMING, *Uniqueness results in an extension of Pauli’s phase retrieval problem*, Applied and Computational Harmonic Analysis, 37 (2014), pp. 413–441.
- [20] J. LI AND T. ZHOU, *On relaxed averaged alternating reflections (RAAR) algorithm for phase retrieval with structured illumination*, Inverse Problems, 33 (2017), p. 025012.
- [21] D. R. LUKE, *Relaxed averaged alternating reflections for diffraction imaging*, Inverse problems, 21 (2004),

- p. 37.
- [22] Z. PRUŠA AND P. L. SØNDERGAARD, *Real-time spectrogram inversion using phase gradient heap integration*, in Proc. Int. Conf. Digital Audio Effects (DAFx-16), 2016, pp. 17–21.
 - [23] P. L. SØNDERGAARD, B. TORRÉSANI, AND P. BALAZS, *The linear time frequency analysis toolbox*, International Journal of Wavelets, Multiresolution and Information Processing, 10 (2012), p. 1250032.
 - [24] M. WELLERSHOFF, *Unknown pleasures: phase retrieval for time-frequency and time-scale structured data*, PhD thesis, ETH Zurich, 2022, <https://www.research-collection.ethz.ch/bitstream/handle/20.500.11850/548828/main.pdf>.